Evaporation of Lennard-Jones fluids

Shengfeng Cheng, Jeremy B. Lechman, Steven J. Plimpton, and Gary S. Grest

Citation: J. Chem. Phys. **134**, 224704 (2011); doi: 10.1063/1.3595260
View online: http://dx.doi.org/10.1063/1.3595260
View Table of Contents: http://jcp.aip.org/resource/1/JCPSA6/v134/i22
Published by the American Institute of Physics.

Evaporation of Lennard-Jones fluids

Shengfeng Cheng,[a] Jeremy B. Lechman, Steven J. Plimpton, and Gary S. Grest
Sandia National Laboratories, Albuquerque, New Mexico 87185, USA

(Received 26 January 2011; accepted 6 May 2011; published online 10 June 2011)

Evaporation and condensation at a liquid/vapor interface are ubiquitous interphase mass and energy transfer phenomena that are still not well understood. We have carried out large scale molecular dynamics simulations of Lennard-Jones (LJ) fluids composed of monomers, dimers, or trimers to investigate these processes with molecular detail. For LJ monomers in contact with a vacuum, the evaporation rate is found to be very high with significant evaporative cooling and an accompanying density gradient in the liquid domain near the liquid/vapor interface. Increasing the chain length to just dimers significantly reduces the evaporation rate. We confirm that mechanical equilibrium plays a key role in determining the evaporation rate and the density and temperature profiles across the liquid/vapor interface. The velocity distributions of evaporated molecules and the evaporation and condensation coefficients are measured and compared to the predictions of an existing model based on kinetic theory of gases. Our results indicate that for both monatomic and polyatomic molecules, the evaporation and condensation coefficients are equal when systems are not far from equilibrium and smaller than one, and decrease with increasing temperature. For the same reduced temperature T/T_c, where T_c is the critical temperature, these two coefficients are higher for LJ dimers and trimers than for monomers, in contrast to the traditional viewpoint that they are close to unity for monatomic molecules and decrease for polyatomic molecules. Furthermore, data for the two coefficients collapse onto a master curve when plotted against a translational length ratio between the liquid and vapor phase. © *2011 American Institute of Physics*. [doi:10.1063/1.3595260]

I. INTRODUCTION

The inverse processes of evaporation and condensation are of fundamental importance in natural phenomena and engineering applications. In both processes, heat and mass transfer between liquid and vapor phases.[1] The key physical quantities to determine are the interphase mass and energy transfer rates. There have been a number of theoretical analyses, using either kinetic theory[1–10] or nonequilibrium thermodynamics,[11–13] to predict these rates as well as the density, temperature, and pressure profiles in the vapor phase. In the framework of kinetic theory of gases, the problem was typically formulated based on the Boltzmann-Bhatnagar-Gross-Krook-Welander (BBGKW) equation for the vapor, with the liquid surface temperature and the temperature, pressure, and velocity of vapor far away from the interface as boundary conditions. To obtain solutions of the BBGKW equation, one further assumption of the liquid/vapor interface was usually made, i.e., all molecules approaching the interface completely condense into the liquid phase, while molecules evaporated from the liquid surface have a Maxwell-Boltzmann (MB) velocity distribution corresponding to the saturated vapor at the liquid temperature. This is equivalent to assuming that the evaporation and condensation coefficients are unity since the evaporation (condensation) coefficient is defined as the ratio of an experimental evaporation (condensation) rate to a theoretical maximum rate given by the Hertz-Knudsen (HK) equation, which is exactly the rate corresponding to a MB distribution. Though the evaporation and condensation coefficients are closely related and have the same value for an interface in equilibrium, they could be substantially smaller than unity and have different values for nonequilibrium interfaces. The above assumption of the boundary condition at the liquid/vapor interface might not be realistic and recently some theoretical work emerged attempting to replace it with more physical ones.[14–18]

The kinetic theory of evaporation and condensation was challenged in a recent experiment of Fang and Ward.[19] They measured the temperature profile to within one mean free path ($\sim 19\,\mu$m) of the interface of an evaporating liquid and found a discontinuity in temperature across the interface that was much larger in magnitude and in the opposite direction to that predicted by the kinetic theory or nonequilibrium thermodynamics. This disagreement led Fang and Ward to conclude that the boundary conditions traditionally assumed for the BBGKW equation were unphysical and they developed a statistical rate theory of evaporation flux to explain their experimental observations.[20,21]

To elucidate the physics of the liquid/vapor interface during evaporation and condensation, more detailed measurements are still needed at even smaller scales and with more refined resolutions. However, the liquid/vapor interface is difficult to probe experimentally and available data can only provide limited information of the microscopic detail of an evaporating interface. In the past several decades, although many measurements have been reported on the evaporation and condensation coefficients of various materials, it still remains unclear how these results can be related to the molecular processes occurring at the liquid/vapor interface. Furthermore, reported values are often scattered in such a large range

[a]Electronic mail: sncheng@sandia.gov.

even for the same material, which further complicates their theoretical interpretation. For example, the reported measurements of the evaporation coefficient of water range from 0.01 to 1.0,[22,23] which exemplifies the difficulty to obtain accurate values of these coefficients, let alone the molecular mechanism of evaporation and condensation.

The development of computer simulation techniques, particularly the molecular dynamics (MD) method, has enabled a number of studies of the evaporation and condensation processes at the molecular scale,[16,17,24–38] which have advanced substantially our understanding of these interphase mass and energy transfer phenomena. Matsumoto *et al.* studied the liquid/vapor interfaces of argon, water, and methanol, and obtained the evaporation and condensation coefficients that agree reasonably well with experimental values.[24–28] Tsuruta *et al.* studied the condensation coefficient of Lennard-Jones (LJ) fluids by injecting test molecules to bombard the liquid/vapor interface and measured the reflecting probability, from which the condensation coefficient was deduced.[29–32] Their results confirmed that the evaporation and condensation coefficients are equal in equilibrium systems, but revealed that the condensation probability generally depends on the normal component of the kinetic energy of incident molecules. This is in contrast to the common assumption that the condensation probability is constant for vapor molecules that hit the liquid surface. They also measured the velocity distributions of the evaporated and reflected molecules at the liquid/vapor interface. Inspired by the MD results, Tsuruta *et al.* developed an expression for the velocity-dependent condensation probability and later justified this expression using the transition state theory,[30,31] which was used earlier to estimate the condensation coefficient by Fujikawa and Maerefat.[39] Anisimov *et al.* also used MD to investigate the evaporation of LJ fluids and the properties of liquid/vapor interfaces, and extended their studies to the case of high-rate evaporation.[33,34]

Recently, Rosjorde *et al.* used MD simulations to study LJ/spline fluids and found evidence for the hypothesis of local equilibrium at a liquid/vapor interface.[35,36] They also measured transfer coefficients of the mass and energy fluxes and found that they agree with kinetic theory from the triple point to about halfway to the critical point. They suspected that the disagreement between kinetic theory predictions and experimental results of Fang and Ward was due to the fact that the theory dealt with monatomic fluids, while in the experiment polyatomic fluids were used. Meland *et al.* also studied LJ/spline fluids and compared their MD results with gas-kinetic calculations.[37] They found that the evaporation and condensation coefficients are not equal outside equilibrium and there is a significant drift velocity in the distribution function at the interphase for both net evaporation and net condensation. Ishiyama *et al.* used MD simulations of LJ fluids to check the validity of kinetic boundary conditions for the BBGKW equation and found that the condensation coefficient is close to unity below the triple-point temperature and decreases gradually as the temperature rises.[38]

More recently, Holyst and Litniewski studied the evaporation of nanodroplets and demonstrated that the evaporation process is limited by the heat transfer and energy balance condition.[16] This finding challenges the basic assumption of kinetic theory that the evaporation flux is determined by the diffusion of mass in the vapor phase. In another study, they simulated a LJ liquid film evaporating into a vacuum and measured the density, temperature, and pressure profiles.[17] Holyst and Litniewski found that mechanical equilibrium is established very quickly and derived an expression for the mass flux that described their simulation results much better than the frequently used HK formula.

In these previous studies, only simple LJ fluids composed of monomers were used. However, it is well known that the vapor pressure of a LJ fluid is much higher than those of real liquids. Though a high vapor pressure implies that LJ liquids are relatively easy to evaporate, it does not necessarily mean that the evaporation coefficient is close to unity because the corresponding theoretical maximum flux is also large. In fact, some previous simulations found that at a moderate temperature the evaporation and condensation coefficients for simple LJ liquids are around 0.8.[27,30,36]

In this paper, we first simulate the evaporation of LJ monomers and then extend MD simulations to the evaporation of LJ fluids composed of dimers and trimers. This allows us to examine the effect of molecular composition on the evaporation rate and the evaporation and condensation coefficients. The paper is organized as follows. In Sec. II, the simulation methodology and the procedure for creating the liquid/vapor interface and removing atoms to implement controlled evaporation are introduced. Results on phase diagrams and surface tensions of dimers and trimers are presented in Sec. III. In Sec. IV results on density and temperature profiles are presented. The measured evaporation rates are found to agree well with the modified HK expression derived by Holyst and Litniewski.[17] The role of mechanical equilibrium during evaporation is also examined. Then in Sec. V we measure the velocity distributions of the evaporated and condensed molecules and compare them to predictions of a kinetic model of evaporation based on the transition state theory of Tsuruta *et al.*[29–32] The evaporation and condensation coefficients are also determined. A brief summary and conclusions are included in Sec. VI.

II. SIMULATION METHODOLOGY

We carried out large scale MD simulations of three simple liquids. In all three cases the interaction between atoms is described by the standard LJ 12-6 potential,

$$U(r) = 4\epsilon[(\sigma/r)^{12} - (\sigma/r)^6 - (\sigma/r_c)^{12} + (\sigma/r_c)^6], \qquad (1)$$

where r is the distance between two atoms, ϵ is the unit of energy, and σ is the diameter of the atom. The interaction is truncated at $r_c = 2.5\sigma$. While commonly used to simulate liquids, the LJ model has one serious drawback when modeling the evaporation process. Namely it has a very high vapor pressure. This results in a very large vapor density which does not match the properties of most liquids. One simple way to make the model more realistic but still retain the simplicity of the LJ interaction is to model the liquid as short chains of LJ atoms. In this paper we show that by modeling dimers that consist of two atoms and trimers consisting of a linear

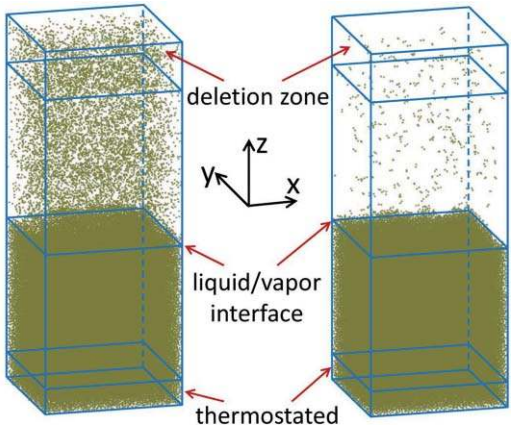

FIG. 1. Liquid/vapor equilibrium at $T = 0.9\epsilon/k_B$ for LJ monomers (left) and dimers (right). The vapor density is clearly lower for dimers.

chain of three atoms, we obtain a more reasonable low vapor density. In dimer and trimer molecules, the bonded atoms are connected by an additional finitely extensible nonlinear elastic (FENE) potential,

$$U_{\mathrm{FENE}}(r) = -\frac{1}{2}kR_0^2 \ln[1-(r/R_0)^2], \tag{2}$$

where $k = 30k_BT/\sigma^2$, T is the temperature, k_B is the Boltzmann constant, and $R_0 = 1.5\sigma$.[40]

All MD simulations were performed using the LAMMPS simulation package.[41] Each system started with $N = 3\,000\,000$ atoms in a parallelepiped of dimensions $L_x \times L_y \times L_z$, where $L_x = L_y = 200\sigma$. The simulation cell was periodic in the x and y directions and had upper and lower confining walls in the z direction as illustrated in Fig. 1. Both upper and lower z-walls interacted with the monomers with a LJ 9-3 potential, which depends only on the distance z from the wall,

$$U(z) = \epsilon_w\left[\frac{2}{15}(\sigma/z)^9 - (\sigma/z)^3 - \frac{2}{15}(\sigma/z_c)^9 + (\sigma/z_c)^3\right], \tag{3}$$

where $\epsilon_w = 2\epsilon$. At the lower wall the interaction was truncated at $z_c = 2.5\sigma$, while at the upper wall it was purely repulsive with $z_c = 0.72\sigma$. Each liquid film was constructed by placing N atoms randomly in the simulation cell with L_z chosen so that the system was near its bulk liquid density. Overlaps were removed by running a short simulation with the "nve/limit" option in LAMMPS enabled.[42] This limits the maximum displacement of an atom per time step and is an efficient way to remove overlaps between atoms. The system was then equilibrated at pressure $P = 0$ by adjusting the position of the upper wall. After the equilibration, the position of the upper wall was increased by at least 50σ to form a liquid/vapor interface as shown in Fig. 1. The system was then allowed to come to equilibrium with its vapor before the evaporation process was initiated.

The equations of motion were integrated using a velocity-Verlet algorithm with a time step $\delta t = 0.005\tau$ for the dimers and trimers and 0.01τ for the monomers, where $\tau = \sigma(m/\epsilon)^{1/2}$ and m is the monomer mass. However, in simulations to investigate the mechanical equilibrium during evaporation, the time step was reduced to 0.001τ in order to get the small pressures accurate in the liquid phase. During the equilibration, T was held constant by a Langevin thermostat weakly coupled to all atoms with a damping constant $\Gamma = 0.1\tau^{-1}$. Once the liquid/vapor interface was equilibrated, the Langevin thermostat was removed except for those atoms within 15σ of the lower boundary at $z = 0$. We refer to the liquid temperature in this region as the bulk temperature T_b. The system was then equilibrated for an additional 20 000 to 100 000 time steps before the evaporation process was initiated.

To model evaporation, a deletion zone of thickness 20σ approximately 50σ above the starting liquid/vapor interface was defined where atoms were removed at a specified rate. For dimer and trimer systems, when the first atom from a molecule was removed, the entire molecule was removed. In this paper, the evaporation rate is defined as the number of atoms removed per unit time and area. Therefore, one removed dimer (trimer) molecule contributes two (three) evaporated atoms. In simulations with a controlled evaporation rate, n atoms in the deletion zone were removed every N_t time steps. Typically, $n = 10$ and $N_t = 100$ or 1000 for monomers and dimers. Since each trimer molecule contains 3 atoms, setting $n = 9$ and $N_t = 90$ or 900 for trimer systems ensured the same evaporation rates as for the other two systems. By removing all atoms that entered the deletion zone, a system in contact with a vacuum was effectively modeled. Since only those atoms within 15σ of the lower wall were coupled to the thermostat, the thermostat did not affect the evaporation process at the liquid/vapor interface. To avoid any finite size effects we only analyzed evaporation data for films thicknesses larger than $\sim 50\sigma$.

In our simulations, the density and temperature profiles in the simulation cell were measured. For liquid/vapor equilibrium cases, time-averages of the density and surface tension were calculated to determine the liquid/vapor phase diagrams. For systems undergoing evaporation, instantaneous density and temperature distributions were calculated. Since these systems are translationally invariant in the x-y plane, both quantities only depend on z and results presented here were averaged over x and y directions.

The meaning and definition of temperature in non-equilibrium systems still have many ambiguities.[43] In this paper, we measured a local temperature $T(z)$ in two ways. In one, $T(z)$ is taken as the mean kinetic energy of atoms locating in the spacial region from $z - \Delta z$ to $z + \Delta z$, where Δz is typically 0.5σ. The corresponding expression is

$$T(z) = \frac{m}{3N_l k_B}\sum_{z-\Delta z}^{z+\Delta z} v^2, \tag{4}$$

where N_l is the number of atoms in the region and v is the atomic velocity. Another definition of the local temperature is based on velocities relative to the possible advective motion induced by evaporation and can be written as

$$T_r(z) = \frac{m}{3N_l k_B}\sum_{z-\Delta z}^{z+\Delta z} (v-\overline{v})^2, \tag{5}$$

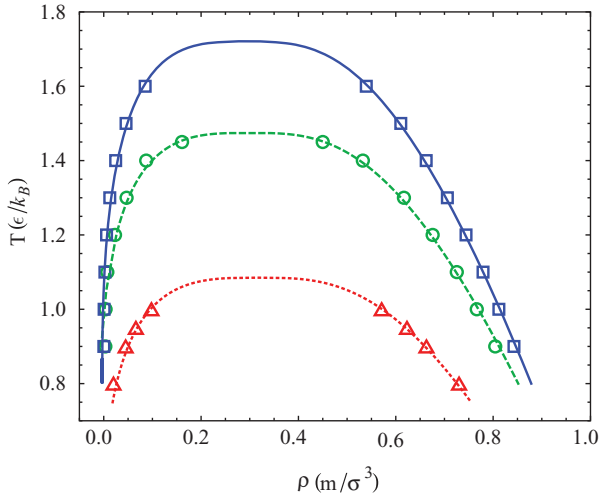

FIG. 2. Liquid/vapor phase diagram for LJ monomers (triangles), dimers (circles), and trimers (squares).

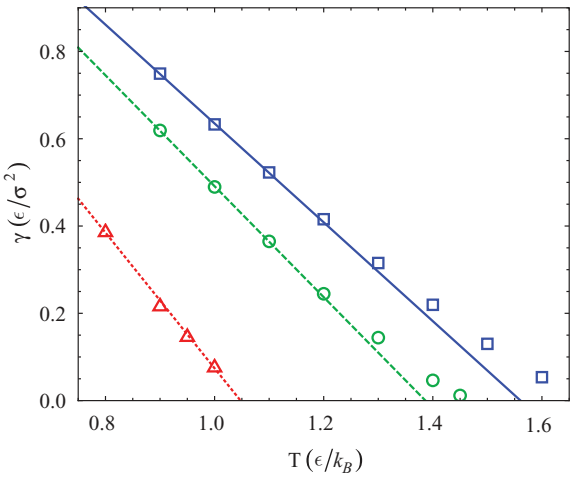

FIG. 3. Surface tension γ as a function of temperature for LJ monomers (triangles), dimers (circles), and trimers (squares). The results for monomers are taken from Ref. 50.

where $\overline{v}$ is the mean atomic velocity in the spatial region from $z - \Delta z$ to $z + \Delta z$. Clearly, the two definitions give identical results in equilibrium since $\overline{v} = 0$ there. However, the results are generally different in nonequilibrium states. This will be discussed further in Sec. IV.

III. LIQUID/VAPOR EQUILIBRIUM

For the system composed of LJ monomers, the liquid/vapor phase diagram is well known.[44–51] However, this is not the case for dimers and trimers. Therefore for these two systems we also simulated the liquid/vapor coexistence by removing the walls in the z direction and replacing them with periodic boundary conditions, which resulted in two liquid/vapor interfaces in the simulation cell. The liquid and vapor densities ρ_L and ρ_V respectively along the coexistence curve for all three systems are shown in Fig. 2. The liquid/vapor critical temperature T_c for each system is determined from fitting the measured densities to

$$\begin{aligned} \rho_L + \rho_V &= a - bT, \\ \rho_L - \rho_V &= A(1 - T/T_c)^{\beta'}, \end{aligned} \tag{6}$$

where a, b, and A are fitting parameters.[45] The critical exponent $\beta' = 0.318$ is for Ising systems that are in the same universality class as simple fluids; thus it is fixed to this value in the fitting. The best fits using Eq. (6) give the critical temperature $T_c = 1.085$, 1.475, and $1.720\epsilon/k_B$, and the critical density $\rho_c = 0.316$, 0.299, and $0.294m/\sigma^3$ for the monomer, dimer, and trimer systems, respectively.

The surface tension of the liquid/vapor interface was determined by measuring the stress tensor. Since the two interfaces are parallel to the x-y plane, the surface tension γ is given by the Kirkwood-Buff formula,[52]

$$\begin{aligned} \gamma &= \frac{1}{2}\int_0^{L_z} [p_{zz}(z) - (p_{xx}(z) + p_{yy}(z))/2]\mathrm{d}z \\ &= \frac{L_z}{2}[P_z - (P_x + P_y)/2], \end{aligned} \tag{7}$$

where $p_{xx}(z)$, $p_{yy}(z)$, and $p_{zz}(z)$ are the three diagonal components of the stress tensor, and P_x, P_y, and P_z are the spatially averaged pressure in each direction. The factor $1/2$ before the integral comes from the fact that there are two interfaces. Far from the liquid/vapor interface, both the liquid and vapor phases are homogeneous and isotropic, and all diagonal components of the stress tensor are the same and equal to the hydrostatic pressure. Therefore in these regions the integrand in Eq. (7) is zero and does not contribute to the integral. Near the interface whose normal is along the z-direction, $p_{xx}(z)$ and $p_{yy}(z)$ are less than $p_{zz}(z)$, leading to a difference in P_x, P_y, and P_z. The net outcome is a nonzero surface tension of the liquid/vapor interface. Results for γ are shown in Fig. 3 for LJ monomers, dimers, and trimers. As expected, γ drops as temperature is raised and approaches zero as T_c is reached. When the temperature T is well below T_c, the surface tension γ roughly decreases linearly with T. However, when T_c is approached the rate of reduction of γ becomes smaller. It is expected $\gamma \sim (T_c - T)^{\nu}$ with ν as a critical exponent. Results in Fig. 3 are consistent with $\nu > 1$.[53]

Figure 3 also shows that the surface tension is smaller for monomers and larger for dimers and trimers. This implies that the cohesion between molecules becomes stronger as the chain length gets longer. Accordingly, at the same temperature the vapor densities of dimers and trimers are lower than that of monomers, as illustrated in Fig. 1. Note that dimers and trimers considered in this paper are very flexible objects. It is not surprising that longer chains lead to stronger attractive interactions between molecules because there are more interacting sites and the counteractive effect of rotational degrees of freedom is suppressed. We will see later that the stronger cohesion in dimers and trimers also affects their evaporation and condensation coefficients.

IV. EVAPORATION OF LENNARD-JONES FLUIDS

A. Monomers

When placed in contact with a vacuum, the evaporation of the LJ monomer system occurs very rapidly, as shown in

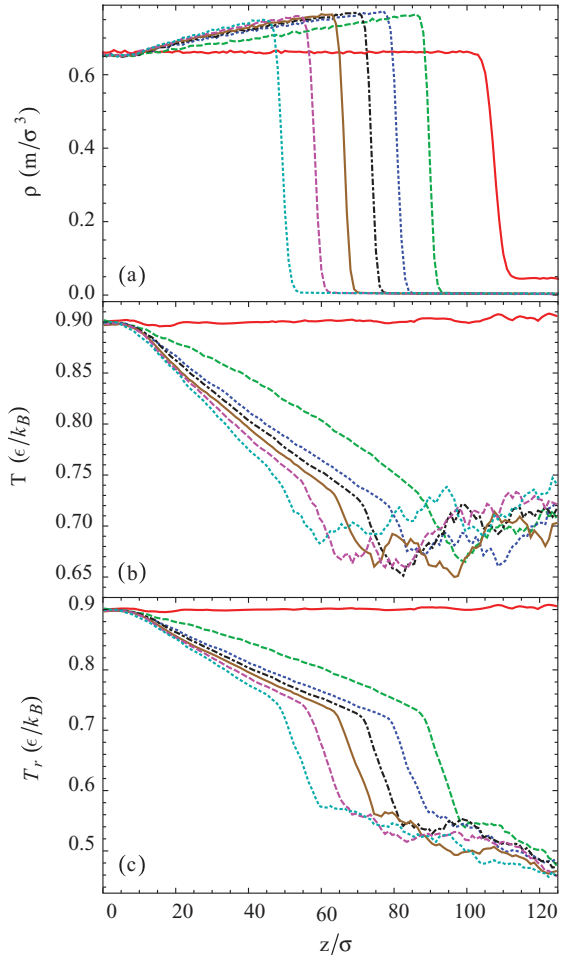

FIG. 4. (a) Density, (b) temperature [defined as the average kinetic energy, Eq. (4)], and (c) temperature [with mean velocity subtracted, Eq. (5)] for a LJ monomer fluid at $T_b = 0.9\epsilon/k_B$ in contact with a vacuum. From right to left the profiles are plotted every 2000τ since the evaporation process was started at $t = 0$ (the rightmost curve).

Fig. 4(a). The vapor is quickly depleted and the vapor density drops by an order of magnitude from its equilibrium value. The liquid density increases by about 20% from its equilibrium value near the interface[17] as there is significant evaporative cooling of the liquid film [Figs. 4(b) and 4(c)], no matter the temperature is measured either as $T(z)$ in Eq. (4) or as $T_r(z)$ in Eq. (5). Note that there is essentially no advective motion in the liquid region, and thus $\bar{v} = 0$ and $T(z) = T_r(z)$ there. However, since the vapor is very dilute when in contact with a vacuum, all molecules leaving the liquid phase almost move freely toward the deletion zone and get removed. As a consequence of the absence of collision, the vapor region is far from local equilibrium and the mean velocity $\bar{v}$ is of order $\sqrt{k_B T/m}$. Therefore $T(z)$ is very different from $T_r(z)$ in the vapor phase, as shown in Figs. 4(b) and 4(c).

Though $T(z)$ and $T_r(z)$ are quite different in the vapor phase when in contact with a vacuum, they are the same in the liquid region in all cases. They are also very close in both the liquid and vapor regions in our other simulations described later where the evaporation rate is controlled and the vapor density during evaporation remains comparable to its equilibrium value. From an experimental perspective, it is the average kinetic energy that is measured when a thermocouple is placed in the vapor phase during evaporation. With these considerations, we refer to $T(z)$ as *temperature* in this paper and report its measurements hereafter. Holyst and Litniewski[17] called this temperature the *pseudotemperature* and concluded that it is very useful in describing the evaporation kinetics.

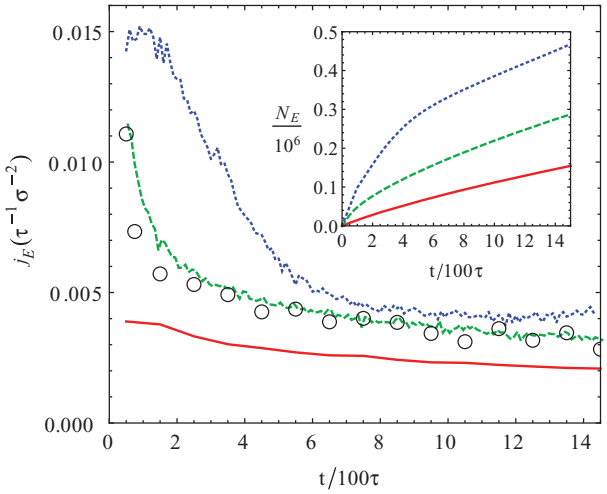

FIG. 5. Evaporation rate j_E vs. time for a monomer system in contact with a vacuum at $T_b = 0.8$ (solid line), 0.9 (dashed line), and $1.0\epsilon/k_B$ (dotted line). The predicted evaporation flux j_m/m based on Eq. (9) is shown as circles. The inset shows the total number of removed atoms N_E vs. time.

Figure 4 shows that both the density and temperature gradients increase as the evaporation process continues. After a short time, the temperature has decreased across the interface from its initial value of $0.9\epsilon/k_B$ to around $0.7\epsilon/k_B$, which is very close to the triple-point temperature of this system.[47] Similar results were found for $T_b = 0.8\epsilon/k_B$ and $1.0\epsilon/k_B$, where the temperature at the liquid/vapor interface also drops to $\sim 0.7\epsilon/k_B$. The large increase in density and decrease in temperature near the interface reported here for LJ monomers are much stronger than those of most common fluids such as water. In this sense, the particular feature of LJ model makes the effect of evaporation more dramatic. The density enhancement near an evaporating interface was also observed in the simulations of Holyst and Litniewski.[17]

An evaporation rate j_E is defined as the number of atoms removed in the deletion zone per unit time and area. It is related to the total number N_E of removed atoms through

$$j_E = \frac{1}{L_x L_y}\frac{dN_E}{dt}. \tag{8}$$

Results for j_E and N_E are shown in Fig. 5 for LJ monomers at three temperatures. As expected, j_E is larger at higher T_b since evaporation is a thermally activated process and occurs more rapidly at higher temperature. The rate j_E also shows strong time dependence. In all cases, j_E initially has a high value since the LJ fluid has a high vapor density and there are plenty of vapor molecules entering the deletion zone. As the vapor is rapidly depleted, j_E drops significantly over time and eventually reaches a plateau. The final reduction factor, defined as the ratio between the value of j_E at $t = 0$ when the evaporation was initiated and that at very large t, is about 2

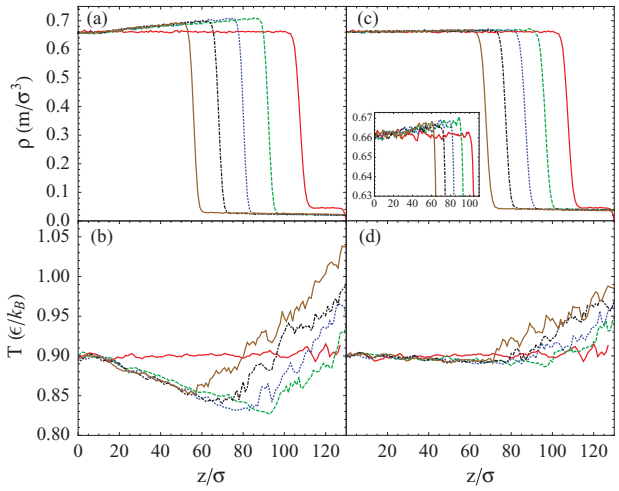

FIG. 6. Density [(a) and (c)] and temperature [(b) and (d)] for a LJ monomer fluid at $T_b = 0.9\epsilon/k_B$ evaporating at a rate $j_E = 1.0 \times 10^{-3}\tau^{-1}\sigma^{-2}$ [(a) and (b)] or $j_E = 2.5 \times 10^{-4}\tau^{-1}\sigma^{-2}$ [(c) and (d)]. From right to left the profiles are plotted every 8000τ [(a) and (b)] or $24\,000\tau$ [(c) and (d)] since the evaporation process was started at $t = 0$ (the rightmost curve). The inset in (c) shows a blowup of the density in the liquid and interfacial region.

for $T_b = 0.8\epsilon/k_B$ and increases to about 4 for $T_b = 0.9\epsilon/k_B$ and $1.0\epsilon/k_B$.

Holyst and Litniewski demonstrated that during evaporation of a liquid film into a vacuum the momentum flux, $j_p \equiv n_{vap} M \langle u_z^2 \rangle$, in the vapor phase far from the liquid/vapor interface, is equal to the pressure in the liquid film, p_{liq}.[17] Here n_{vap} is the vapor number density, M is the molecular mass, and $\langle u_z^2 \rangle$ is the mean squared z component of the molecular velocity. From this observation they proposed an equation for the mass flux during evaporation,

$$j_m \equiv n_{vap} M \langle u_z \rangle = p_{liq} \frac{\langle u_z \rangle}{\langle u_z^2 \rangle}, \tag{9}$$

where $\langle u_z \rangle$ is the mean z component of the molecular velocity. Note that j_m has the unit of mj_E. In our simulations, p_{liq}, $\langle u_z \rangle$, and $\langle u_z^2 \rangle$ are averaged in a thin region from $z_{int}(t) + z_1$ to $z_{int}(t) + z_2$, where $z_{int}(t)$ denotes the location of interface at time t. Typically, $z_1 = -30\sigma$ and $z_2 = -10\sigma$ for p_{liq}, and $z_1 = 20\sigma$ and $z_2 = 40\sigma$ for $\langle u_z \rangle$ and $\langle u_z^2 \rangle$. However, results are not sensitive to the exact location of these regions and vary by a few percent at most as long as they are far from the liquid/vapor interface. The calculated mass flux j_m from the above equation at $T_b = 0.9\epsilon/k_B$ is shown in Fig. 5. Clearly, the measured j_E agrees with j_m/m at most times, except at the beginning stage of evaporation when j_m/m tends to be a few percent smaller than j_E.

We also ran simulations in which j_E was controlled by limiting the number of atoms removed from the deletion zone during a given simulation period. Results for the density and temperature profiles are shown in Fig. 6 for two rates that are smaller than the final evaporation rate in the case of contacting with a vacuum, the plateau in Fig. 5, by a factor around 4 and 16, respectively. In Figs. 6(a) and 6(b), the density enhancement and temperature drop are still clearly visible, but the magnitudes are greatly reduced compared with those in Fig. 4. The vapor density in this case is also reduced from the equilibrium value but remains finite. For a very slow evaporation rate [Figs. 6(c) and 6(d)], these two effects almost disappear and the vapor density is close to the equilibrium density.

In addition to the evaporative cooling, the temperature profiles shown here [Figs. 4(b), 6(b), and 6(d)] indicate that the temperature of vapor increases with the distance from the liquid/vapor interface. This can be understood by a simple argument: molecules with higher kinetic energies evaporate faster and more energetic molecules accumulate near the deletion zone, leading to a higher temperature at this end and a temperature gradient in the vapor phase. Therefore, if the vapor temperature is measured at a certain distance away from the liquid/vapor interface, it will be higher than the actual temperature at the interface. This phenomenon is qualitatively consistent with the experimental measurement by Fang and Ward.[19] They measured the temperature at locations as close as one mean free path of the interface of an evaporating liquid and the results indicated that the vapor temperature is indeed greater than that in the liquid phase at the interface. They also concluded this is due to more energetic molecules that are likely to evaporate first. Note that the experimental condition in Ref. 19 is close to the situation where the evaporation rate is controlled here. In this case, the vapor density is generally large enough to make local thermal equilibrium approximately true. Our simulations confirmed that the mean velocity $\bar{v}$ is much smaller than $\sqrt{k_B T/m}$, which leads to $T(z) \simeq T_r(z)$. Since the temperature recorded by the thermocouple is related to the average kinetic energy of vapor molecules, the qualitative comparison made here between simulations and experiments should be reasonable.

B. Dimers and trimers

While the LJ potential serves as a reasonable approximation of nonbonded interatomic interactions, most liquids of interest are composed of molecules not single atoms. One simple extension is to consider molecules of two or more LJ monomers bound together. In the present simulations, the bonded interaction is realized through the introduction of a FENE potential [Eq. (2)] between bonded monomers. The nonbonded interatomic interactions are still given by the LJ potential [Eq. (1)].

Results on the density and temperature profiles for the LJ dimer system in contact with a vacuum or evaporating at a controlled evaporation rate are shown in Fig. 7 for $T_b = 1.2\epsilon/k_B$. Those for the trimer system at the same bulk temperature but at two controlled rates are shown in Fig. 9. Results on the evaporation rate j_E at various temperatures when in contact with a vacuum are shown in Fig. 8 (dimer) and Fig. 10 (trimer).

The phenomenology of evaporation into a vacuum for dimers [Figs. 7(a) and 7(b)] and trimers (not shown) is similar to that of monomers, including the density enhancement and the evaporative cooling near the liquid/vapor interface. However, the relative magnitudes of density increase and temperature drop are smaller for dimers and even smaller for

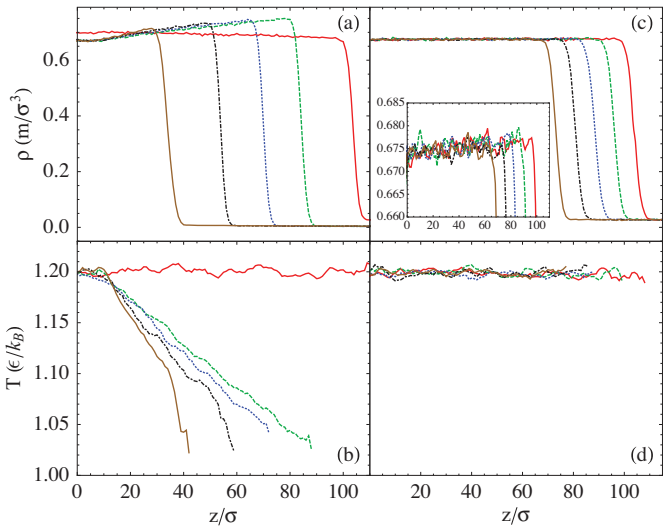

FIG. 7. Density [(a) and (c)] and temperature [(b) and (d)] for the LJ dimer fluid at $T_b = 1.2\epsilon/k_B$ in contact with a vacuum [(a) and (b)] or evaporating at a controlled rate $j_E = 5.0 \times 10^{-5}\tau^{-1}\sigma^{-2}$ [(c) and (d)]. From right to left the profiles are plotted every 5000τ [(a) and (b)] and $100\,000\tau$ [(c) and (d)] since the evaporation process was started at $t = 0$ (the rightmost curve). The inset in (c) blows up the density profile in the liquid and interfacial region. Temperature in the vapor region is not included because the density of vapor is small and the data are too noisy to indicate a clear trend.

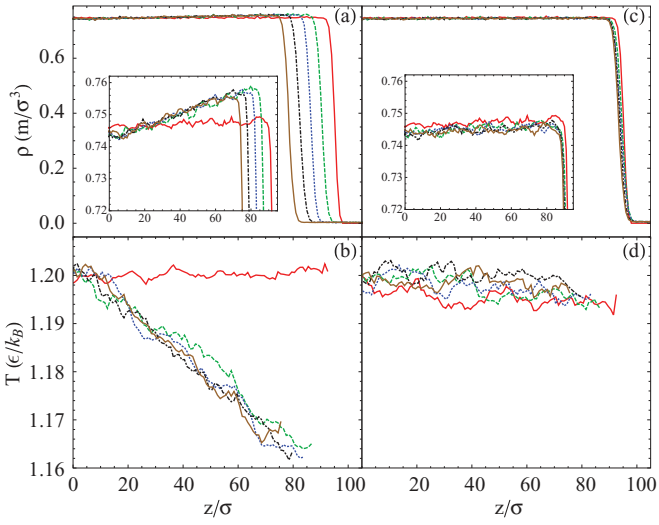

FIG. 9. Density [(a) and (c)] and temperature [(b) and (d)] for the LJ trimer fluid at $T_b = 1.2\epsilon/k_B$ evaporating at a rate $j_E = 5.0 \times 10^{-4}\tau^{-1}\sigma^{-2}$ [(a) and (b)] or $j_E = 5.0 \times 10^{-5}\tau^{-1}\sigma^{-2}$ [(c) and (d)]. From right to left the profiles are plotted every $60\,000\tau$ in both cases since the evaporation process was started at $t = 0$ (the rightmost curve). The insets in (a) and (c) show blowups of density in the liquid and interfacial region.

trimers. This is consistent with the observation that cohesion gets stronger and evaporation slows down in dimer and trimer fluids.

More quantitative information of evaporation into a vacuum is obtained by measuring the evaporation rate j_E. It generally decreases with time and only approaches a constant value after a certain interval. Compared with monomers the reduction factor is smaller for dimers. For the trimer system the time-dependence is weak except near the critical temperature T_c. This is understandable because the vapor density decreases as the chain length increases. As expected, j_E is higher at higher T_b. At the same bulk temperature T_b, j_E is largest for the monomer system and smallest for the trimer. For example, at $T_b = 0.9\epsilon/k_B$ it is around $2 \times 10^{-3}\tau^{-1}\sigma^{-2}$ for monomers, $4 \times 10^{-4}\tau^{-1}\sigma^{-2}$ for dimers, and $4 \times 10^{-5}\tau^{-1}\sigma^{-2}$ for trimers. Thus increasing the number of atoms in a molecule only from 1 to 3 results in a decrease by a factor of more than 50 in j_E.

The results for j_m/m from Eq. (9) for dimers at $T_b = 1.2\epsilon/k_B$ and for trimers at $T_b = 1.2\epsilon/k_B$ and $1.5\epsilon/k_B$ are shown in Figs. 8 and 10, respectively. In all cases, the agreement between j_m/m and j_E is quite satisfactory, indicating that Eq. (9) is valid not only for monatomic liquids, but also for molecular liquids such as dimers and trimers. We also note that in evaluating $\langle u_z^2 \rangle$ in Eq. (9), molecular velocities should be used.

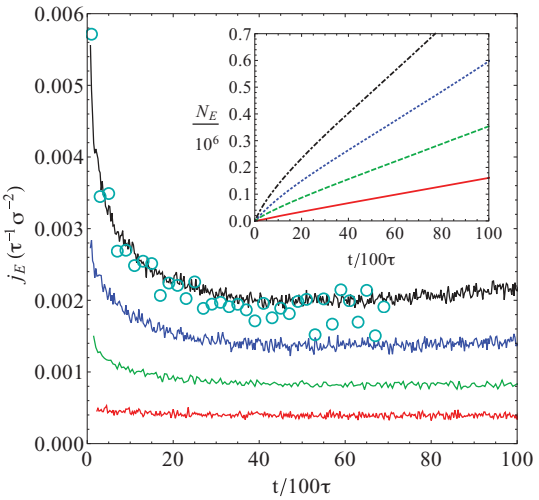

FIG. 8. Evaporation rate j_E vs. time for the LJ dimer system in contact with a vacuum at $T_b = 0.9$, 1.0, 1.1, and $1.2\epsilon/k_B$ (from bottom to top). The predicted evaporation flux j_m/m based on Eq. (9) is shown as circles. The inset shows the total number of removed atoms N_E vs. time.

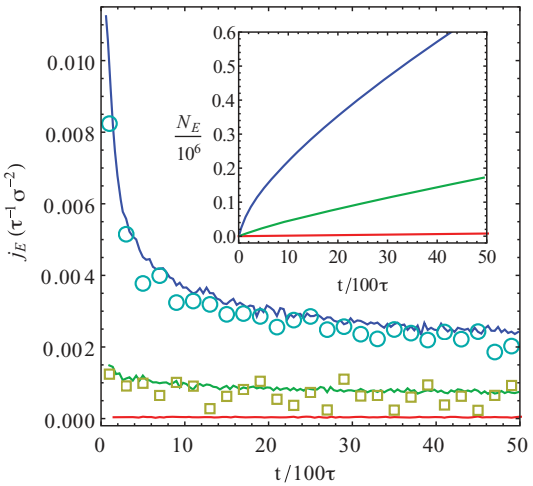

FIG. 10. Evaporation rate j_E vs. time for the LJ trimer system in contact with a vacuum at $T_b = 0.9$, 1.2, and $1.5\epsilon/k_B$ (lines from bottom to top). Open squares and circles show the predicted evaporation flux j_m/m from Eq. (9) at $T_b = 1.2$ and $1.5\epsilon/k_B$, respectively. The inset shows the total number of removed atoms N_E vs. time.

The magnitude of the density enhancement and temperature drop near the interface also depends on the evaporation rate. As shown in Figs. 7(c) and 7(d), for the dimer system at $T_b = 1.2\epsilon/k_B$ they are not observed when j_E is reduced to $5.0 \times 10^{-5}\tau^{-1}\sigma^{-2}$, which is much smaller than the plateau value of j_E of this system in contact with a vacuum. For the trimer system under the same temperature, the density and temperature gradients are visible at $j_E = 5.0 \times 10^{-4}\tau^{-1}\sigma^{-2}$ [Figs. 9(a) and 9(b)], but disappear when j_E is reduced further by a factor of 10 to $j_E = 5.0 \times 10^{-5}\tau^{-1}\sigma^{-2}$ [Figs. 9(c) and 9(d)]. Note that the plateau value of j_E for trimers at this temperature when evaporating into a vacuum is $7.7 \times 10^{-4}\tau^{-1}\sigma^{-2}$. Thus it is reasonable to see density and temperature gradients at $j_E = 5.0 \times 10^{-4}\tau^{-1}\sigma^{-2}$, but not at much slower evaporation rates.

C. Stagnation pressure during evaporation

During evaporation, the vapor escaping into a vacuum is far from equilibrium and a local temperature and pressure defined with respect to a thermodynamic equilibrium cannot be used for its description. Holyst and Litniewski showed that for LJ monomers global quantities, such as total kinetic energy, total mass flux, and total momentum flux, can be well defined and provide useful information about the physical state of the vapor phase.[17] Particularly, a stagnation pressure tensor can be defined as

$$p_{\alpha\beta} = \frac{1}{V}\left(\sum_j m_j v_{j\alpha} v_{j\beta} - \sum_{i>j}\sum_j r_{ij\alpha}\frac{\partial \phi_{ij}}{\partial r_{ij\beta}}\right), \qquad (10)$$

where i and j index all atoms inside the volume V, m_j and v_j are the atomic mass and velocity, r_{ij} and ϕ_{ij} are the interatomic distance and potential, respectively, and Greek indices indicate components along the x, y, and z directions. Note that this pressure tensor is not defined relative to a local equilibrium. Holyst and Litniewski demonstrated that for the stagnation pressure the p_{zz} component in the vapor phase is equal to the liquid pressure, p_{liq}, far from the interface.[17]

We measured the stagnation pressure for Lennard-Jones monomers, dimers, and trimers. Results are shown in Fig. 11. Indeed, for all systems at all times the p_{zz} component in the vapor phase (solid lines in the main panel of Fig. 11) is equal to the pressure in the liquid film (symbols). Data in Fig. 11 are for liquid films evaporating into a vacuum. We confirmed that the equality is also true for systems evaporating at controlled rates.

The inset of Fig. 11 shows the stagnation pressure along the normal direction of the liquid/vapor interface. In the liquid phase, $p_{zz} = p_{xx} = p_{yy} = p_{\text{liq}}$. However, in the vapor phase, $p_{zz} \neq p_{xx} = p_{yy}$, and the difference grows with the distance away from the interface. The inset also shows that the momentum flux, $j_p = n_{\text{vap}} M \langle u_z^2 \rangle$, approaches p_{zz} in the vapor phase far from the interface. This is not surprising for monatomic systems since in this case j_p is exactly the first term in the expression for p_{zz} in Eq. (10). The second term in p_{zz} represents the contribution from interatomic interactions. For systems evaporating into a vacuum, the vapor becomes increasingly dilute away from the liquid/vapor interface so that the contribution to p_{zz} from interactions between two monomers essentially vanishes and the momentum flux dominates. For molecular systems, j_p is not identical to the first term in p_{zz} as expressed in Eq. (10), which is based on atomic velocities not molecular velocities averaged from those of its constitute atoms. However, p_{zz} can be also defined in terms of molecular velocities and the interactions between molecules instead of atoms.[54] Then molecular density becomes dilute during evaporation into a vacuum and the same argument above applies again. The result is that j_p still dominates over the interaction contribution in p_{zz} in molecules escaping into a vacuum. This relation between p_{zz} and j_p in a dilute vapor is the foundation of Eq. (9), from which the mass flux j_m can be determined from p_{liq} since p_{liq} equals p_{zz} in the vapor phase. As shown in Figs. 5, 8, and 10, the agreement between j_m/m and the evaporation rate j_E is very good for all systems evaporating into a vacuum.

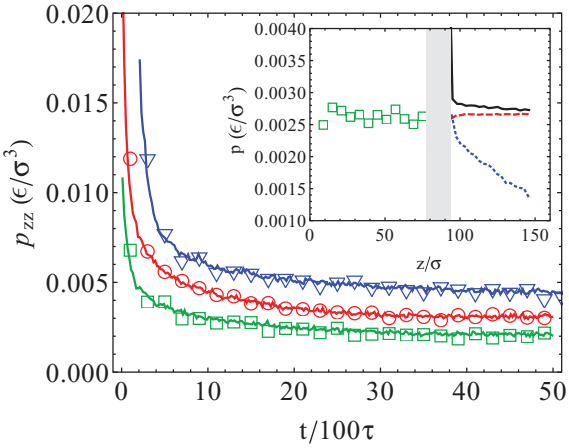

FIG. 11. Stagnation pressure p_{zz} averaged in the liquid phase (symbols) and vapor phase (lines) for: monomers at $T_b = 0.9\epsilon/k_B$ (the middle line and ◯); dimers at $T_b = 1.2\epsilon/k_B$ (the bottom line and □); and trimers at $T_b = 1.5\epsilon/k_B$ (the top line and ▽). The trimer data are shifted upward by $0.002\epsilon/\sigma^3$ and right by 200τ for clarity. The inset shows the stagnation pressure p as a function of distance along the normal direction of the liquid/vapor interface for trimers at $T_b = 1.5\epsilon/k_B$. The pressure in the liquid phase, p_{liq}, is shown as squares (□), and that in the vapor phase, p_{vap}, is shown as the dashed line (the p_{zz} component) and the dotted line [the $(p_{xx} + p_{yy})/2$ component]. The solid line represents the momentum flux $j_p \equiv n_{\text{vap}} M \langle u_z^2 \rangle$. The interfacial region is denoted as a shadowed strip. Data are for systems evaporating into a vacuum.

For systems evaporating at small controlled rates, the vapor density is comparable to its equilibrium value and it is not expected that j_p is equal to p_{zz} even in the vapor phase, though p_{zz} is still equal to p_{liq}. As a result, the mass flux j_m from Eq. (9) is generally different from the evaporation rate mj_E. A simulation of LJ monomers evaporating at $j_E = 1.0 \times 10^{-3}\tau^{-1}\sigma^{-2}$ and $T_b = 0.9\epsilon/k_B$ shows that j_m/m from Eq. (9) is only about 50% of the measured j_E.

V. COMPARISON TO KINETIC THEORY

At the liquid/vapor interface, the molecular exchange between the two phases occurs continuously in the form of evaporation and condensation. Results discussed above show that

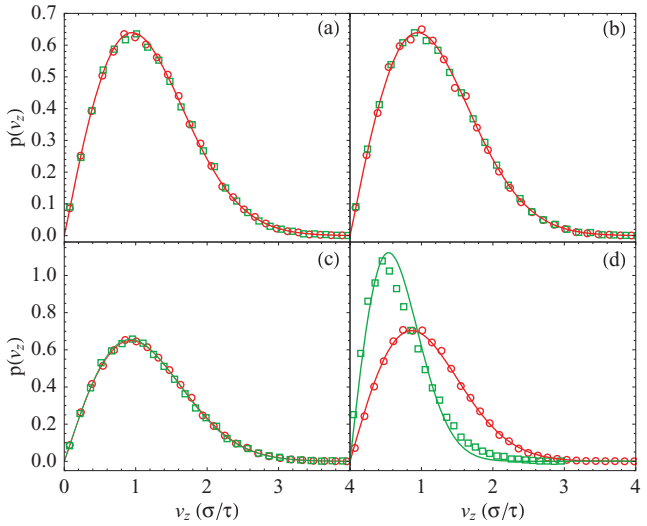

FIG. 12. Velocity distributions of v_z for all molecules that leave (circles) and arrive (squares) at the interface for monomer systems at $T_b = 0.9\epsilon/k_B$ under various evaporation conditions: (a) liquid/vapor equilibrium; (b) controlled rate $j_E = 2.5 \times 10^{-4}\tau^{-1}\sigma^{-2}$; (c) controlled rate $j_E = 1.0 \times 10^{-3}\tau^{-1}\sigma^{-2}$; (d) in contact with a vacuum. Solid lines in (a) and (b) represent the MB distribution with $T_i = T_b = 0.9\epsilon/k_B$. Two solid lines in (c) represent the MB distribution with $T_i = 0.871\epsilon/k_B$ for molecules that leave the interface and $T_i = 0.854\epsilon/k_B$ for molecules that arrive at the interface. Two solid lines in (d) represent the MB distribution with $T_i = 0.744\epsilon/k_B$ for molecules that leave the interface and $T_i = 0.292\epsilon/k_B$ for molecules that arrive at the interface.

the molecular composition affects the evaporation rate to a large extent. It remains an interesting question if the change in molecular composition also affects the atomic kinetics during evaporation and condensation, such as velocity distributions of the molecules. In equilibrium, all molecules leaving the interface to the gas phase or arriving at the interface from the gas phase have a normal velocity v_z that satisfies the MB distribution with a probability density function

$$p(v_z) = \frac{Mv_z}{k_B T_i} \exp\left(-\frac{Mv_z^2}{2k_B T_i}\right), \tag{11}$$

where M is the molecular mass and T_i is the temperature at the interface. Note that T_i equals T_b in equilibrium but is generally lower than T_b when there is net evaporation.

To analyze the velocity distributions, we consider a plane just outside the liquid/vapor transition layer. All molecules crossing this plane and entering (leaving) the transition layer are counted as incoming (outgoing) molecules. Their normal velocity v_z is measured and the corresponding distribution function $p(v_z)$ is calculated. The results for LJ monomers are shown in Fig. 12. Those for dimers and trimers are very similar and are not shown. The results are not sensitive to the position of the plane that molecules cross as long as it is outside but not far, within several σ, from the transition layer.

As expected, Fig. 12(a) shows that when the liquid/vapor interface is in equilibrium the MB distribution is satisfied by molecules that enter or exit the transition layer with a T_i that is the same as the bulk temperature in the liquid and vapor phases. This is also the case when the evaporation rate is as low as $2.5 \times 10^{-4}\tau^{-1}\sigma^{-2}$ [Fig. 12(b)]. When the evaporation rate is increased to $1.0 \times 10^{-3}\tau^{-1}\sigma^{-2}$ [Fig. 12(c)], the MB distribution still holds, but corresponds to a T_i that is slightly lower than T_b, which is fixed by a thermostat near the lower confining wall. Furthermore, in this case slightly different T_i's have to be used for molecules that enter or exit the transition layer.

The situation is quite different in the case of evaporation into a vacuum, where the evaporation rate is very high. Figure 12(d) shows that the velocity distributions of molecules entering or exiting the transition layer have very different T_i's. For the outgoing molecules, $T_i = 0.744\epsilon/k_B$ is consistent with the temperature of the liquid/vapor interface, which is lower than the bulk temperature $T_b = 0.9\epsilon/k_B$ of liquid far from the interface. This reduction of the temperature at the liquid/vapor interface is due to evaporative cooling. For the arriving molecules we found $T_i = 0.292\epsilon/k_B$ when $p(v_z)$ was fit to a MB distribution. This temperature is much lower than that for the outgoing molecules and is only about 1/3 of T_b. The strong asymmetry between T_i's for the outgoing and incoming molecules can be understood as follows. When the liquid evaporates into a vacuum, the vapor density is extremely low and it is very unlikely that a vapor molecule undergoes a collision with other molecules in the vapor phase and is reflected back to the liquid/vapor interface. All molecules leaving the interface tend to move ballistically toward the deletion zone and get removed. This is particularly the case for outgoing molecules with high v_z normal to the interface because they would require multiple collisions to be reflected, which are very rare. Therefore, most reflected molecules are those moving slowly. This leads to a strong imbalance in the distributions of v_z of the incoming and outgoing molecules, which is manifest in the fact that the incoming molecules have a much lower T_i than that of the outgoing molecules.

Results in Fig. 12(d) indicate that if the full velocity distribution is plotted for all the molecules approaching or leaving the liquid/vapor interface, one would expect some deviation from the MB distribution that is symmetric between v_z and $-v_z$. That is, the contribution from positive values of v_z have more weight than that on the negative side. This deviation was also observed in previous MD simulations of evaporation into a vacuum.[15,33] Our results further indicate that this asymmetry also occurs when the evaporation rate is high enough that the vapor density is substantially reduced from its equilibrium value.

Not all molecules arriving at the liquid/vapor interface from the gas phase condense into the liquid phase. A fraction is reflected back into the vapor phase. The condensation coefficient defined in Introduction quantifies this effect. It essentially represents the fraction of incoming molecules that indeed becomes attached to the liquid phase. It has been argued that the condensation coefficient is close to unity for monatomic liquids such as liquid metals,[55] and less than unity for polyatomic liquids because rotational motion of polyatomic molecules in the liquid state makes it more difficult to accommodate newly arriving molecules.[39]

The reflected molecules obviously contribute to the evaporation flux. Equivalently, not all evaporated molecules come directly from the liquid phase. The evaporation coefficient is the ratio between the molecular flux due to real

evaporation, i.e., from those molecules transformed into vapor from the liquid phase, and the maximum flux $j_{\max}$ calculated from the MB distribution. It is easy to derive the HK formula, $j_{\max} = 1/4n\overline{v}$, where n is the density of the saturated vapor at the temperature T_i and $\overline{v}$ is the mean molecular velocity. For liquid/vapor equilibrium the condensation and evaporation coefficients must be the same since the velocity of molecules arriving at the interface also satisfies the MB distribution.

Hereafter, we consider the total evaporation flux as the sum of that due to the true evaporation of liquid molecules and another due to the reflection of incoming vapor molecules. Results in Fig. 12(d) show that when a liquid evaporates into a vacuum, the reflection flux is greatly suppressed because of the depletion of vapor. In this case the total evaporation flux is very close to the true evaporation flux. This is the reason that Ishiyama *et al.* emphasized that the condensation coefficient can be determined without any ambiguity by measuring the spontaneous evaporation flux from the simulations of evaporation into a vacuum.[38]

Through MD simulations of LJ monomers, Tsuruta *et al.* discovered that the condensation coefficient is actually an average quantity.[30–32] For incoming molecules with different normal translational energy $E_{\text{in},z} = Mv_z^2/2$, their tendency to condensate into the liquid phase is generally different. A condensation probability α_c was defined to quantify this tendency and they suggested that α_c depends on the normal velocity of incident molecules in the following functional form,

$$\alpha_c = \alpha\left[1 - \beta\exp\left(\frac{-E_{\text{in},z}}{k_{\text{B}}T_i}\right)\right], \tag{12}$$

where α and β are two parameters that depend on the properties of liquid and temperature. In this framework, the condensation coefficient discussed above is the average of α_c over the velocity distribution of incoming molecules and is denoted as $\overline{\alpha_c}$. Since the velocity of all incoming molecules satisfies a MB distribution, $\overline{\alpha_c}$ can be expressed as

$$\begin{aligned}\overline{\alpha_c} &= \int_0^{+\infty} \alpha_c(v_z)p(v_z)dv_z \\ &= \alpha(1 - \beta/2).\end{aligned} \tag{13}$$

In our simulations we grouped incoming molecules by the normal component v_z of their velocity and measured their condensation probability α_c. However, an ambiguity arises about what incoming molecules should be counted as condensed ones since all molecules arriving at the transition layer will eventually leave after some period of time. We counted as condensed those incoming molecules that stay in the liquid phase or the liquid/vapor transition zone for at least $\Delta t = 25\tau$. Since a typical value of τ is approximately 2ps,[56] Δt is about 50ps. This choice of Δt is somewhat *ad hoc*. However, previous MD simulations have established that the characteristic time of energy excitation during evaporation or energy relaxation during condensation is roughly $50 - 70$ps.[27] For this reason our choice of condensation time scale as 50ps should be reasonable. This choice is further substantiated by the fact that the measured α_c does not change significantly even if Δt is increased by a factor of 2 to 50τ. All data presented here are for $\Delta t = 25\tau$. After α_c was obtained, the

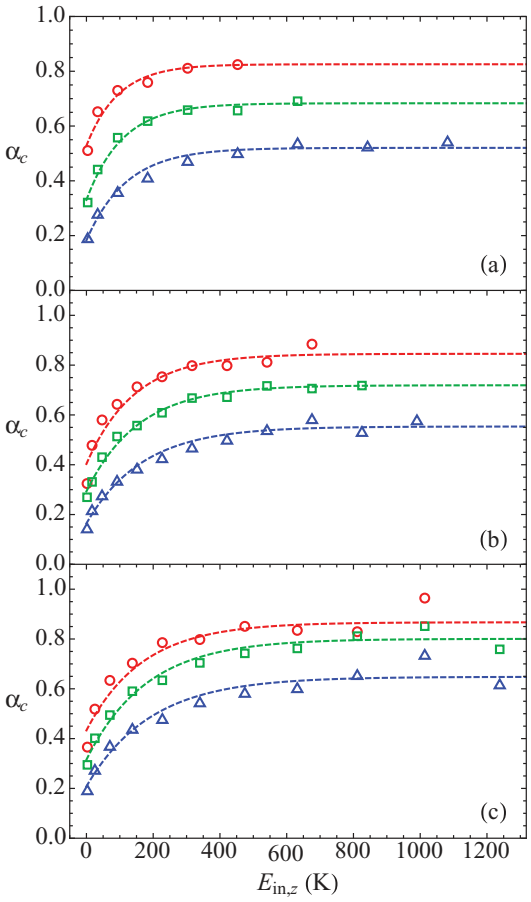

FIG. 13. Condensation probability α_c as a function of $E_{\text{in},z}$, which is the normal component of the translational energy of incoming molecules. Data presented here are measured on liquid/vapor equilibrium systems at various temperatures. However, results are similar if the evaporation rate is fixed at a small value and the liquid/vapor interface is near equilibrium. (a) Monomers; $T_b = 0.8\epsilon/k_{\text{B}}$ (triangles), $0.9\epsilon/k_{\text{B}}$ (squares), and $1.0\epsilon/k_{\text{B}}$ (circles); (b) dimers: $T_b = 1.2\epsilon/k_{\text{B}}$ (triangles), $1.3\epsilon/k_{\text{B}}$ (squares), and $1.4\epsilon/k_{\text{B}}$ (circles); (c) trimers: $T_b = 1.4\epsilon/k_{\text{B}}$ (triangles), $1.5\epsilon/k_{\text{B}}$ (squares), and $1.6\epsilon/k_{\text{B}}$ (circles). In this plot a conversion factor $\epsilon/k_{\text{B}} = 119.8$K (for argon) is used.

$\alpha_c \sim v_z$ was fit to Eq. (12) with α and β as fitting parameters, from which the condensation coefficient $\overline{\alpha_c}$ was calculated using Eq. (13).

Results for $\alpha_c(v_z)$ are shown in Fig. 13. It indicates that α_c indeed follows the functional form in Eq. (12), regardless of the change in molecular composition from monomers to dimers and to trimers. Vapor molecules arriving at the liquid/vapor interface with a small v_z are less likely to condense and join the liquid state. This can be understood with a simple physical picture. When the arriving molecules collide with liquid molecules, they are more likely to be reflected after one or several collisions if their velocity is small. Arriving molecules with a large velocity v_z are able to penetrate the liquid region deeper, and have a bigger chance to survive multiple collisions and to remain in the liquid phase for at least a period $\sim \Delta t$.

The condensation probability α_c being a function of v_z has another implication. Since all molecules leaving the liquid/vapor interface are either those that truly evaporate from the liquid or those that have been reflected, and the velocity of all leaving molecules satisfies the MB distribution (as shown

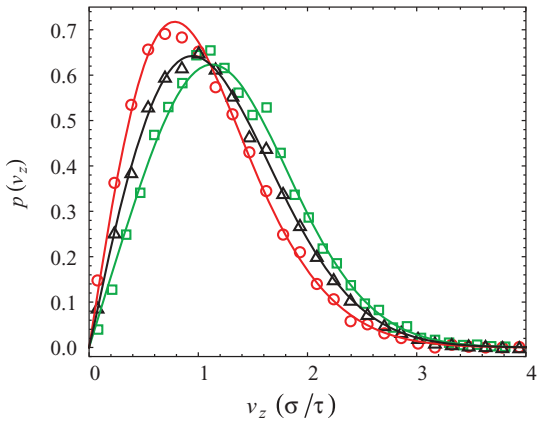

FIG. 14. Velocity distributions of v_z of all molecules, which left (triangles), were evaporated (squares), or were reflected (circles) from the interface for LJ monomers at $T_b = 0.9\epsilon/k_B$ evaporating at a rate $j_E = 2.5 \times 10^{-4}\tau^{-1}\sigma^{-2}$. Solid lines are fits to the MB distribution $p(v_z)$ in Eq. (11) and the modified MB distributions $p_e(v_z)$ and $p_r(v_z)$ in Eqs. (14) and (15), respectively.

in Fig. 12), the normal velocity distributions of the truly evaporated molecules and reflected ones are modified from the MB distribution. Particularly, the MB distribution is modified by the condensation probability α_c for the truly evaporated molecules and by $1-\alpha_c$ for the reflected ones. Thus they have the following forms after a proper normalization,[30]

$$p_e(v_z) = \frac{1-\beta\exp\left(-\frac{Mv_z^2}{2k_BT_i}\right)}{1-\beta/2}\frac{Mv_z}{k_BT_i}\exp\left(-\frac{Mv_z^2}{2k_BT_i}\right), \tag{14}$$

and

$$p_r(v_z) = \frac{1-\alpha+\alpha\beta\exp\left(-\frac{Mv_z^2}{2k_BT_i}\right)}{1-\alpha+\alpha\beta/2}\frac{Mv_z}{k_BT_i}\exp\left(-\frac{Mv_z^2}{2k_BT_i}\right), \tag{15}$$

where the subscripts e and r stand for "truly evaporated" and "reflected", respectively.

The distribution functions $p_e(v_z)$ and $p_r(v_z)$ for the truly evaporated and reflected molecules were measured directly in simulations and provided another way to determine α and β, and eventually the condensation coefficient $\overline{\alpha_c}$. One example is shown in Fig. 14, which includes data on $p(v_z)$, $p_e(v_z)$, and $p_r(v_z)$ of monomers evaporating at a small fixed rate. The successful fits to the MB and modified MB distributions in Eqs. (11), (14), and (15) indicate that the condensation probability α_c provides a reasonable quantitative measure of the condensation and evaporation processes. Furthermore, we compared the condensation coefficient $\overline{\alpha_c}$ determined either using $\alpha_c(v_z)$ or using $p_e(v_z)$ and $p_r(v_z)$. For systems in equilibrium or not far from equilibrium such as evaporation at small controlled rates, the two results generally agree, which further validates the kinetic model of evaporation described above. For systems far from equilibrium such as evaporation into a vacuum, it is generally very difficult to measure $\overline{\alpha_c}$ in these ways because there are essentially no incoming molecules and thus no reflected flux. In this case, it might be possible to determine $\overline{\alpha_c}$ by directly measuring the evaporation flux and comparing it to the theoretical maximum flux j_{max}, as suggested in Ref. 38. However, the temperature of the liquid/vapor interface needs to be determined first in order to calculate j_{max}. This is not an easy task as the interface is moving during evaporation and the temperature is sensitive to the location of measurement in the region around the interface.

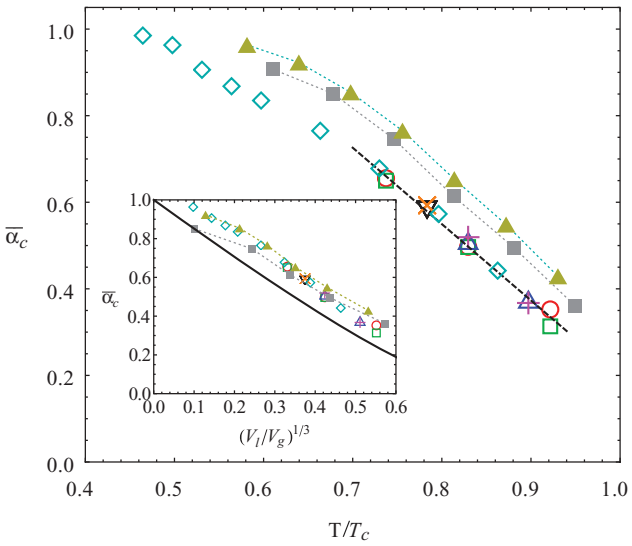

FIG. 15. Condensation coefficient $\overline{\alpha_c}$ vs. temperature for monomers, dimers, and trimers under various evaporation conditions. For monomers: circles (◯) and triangles (△ and ▽) are measured using $\alpha_c(v_z)$; open squares (□), pluses (+), and crosses (×) are measured using $p_e(v_z)$ and $p_r(v_z)$; circles (◯) and open squares (□) are for liquid/vapor equilibrium systems at $T_i = T_b = 0.8\epsilon/k_B$, $0.9\epsilon/k_B$, and $1.0\epsilon/k_B$; upward triangles (△) and pluses (+) are for evaporation rate $j_E = 2.5 \times 10^{-4}\tau^{-1}\sigma^{-2}$ at $T_b = 0.9\epsilon/k_B$ and $1.0\epsilon/k_B$; downward triangles (▽) and crosses (×) are for evaporation rate $j_E = 1.0 \times 10^{-3}\tau^{-1}\sigma^{-2}$ at $T_b = 0.9\epsilon/k_B$. For data measured during evaporation, the actual temperature T_i of the liquid/vapor interface is used. The data for dimers and trimers are shown with solid squares (■) and solid triangles (▲), respectively, and both are calculated using $\alpha_c(v_z)$ from liquid/vapor equilibrium systems. The dashed line is a linear fit to the monomer data at high temperature. The dotted lines are guides to the eye. Our data of LJ monomers agree with those from Ref. 38 [shown with open diamonds (◇)], which were determined by directly measuring the evaporation flux into a vacuum. The inset plots $\overline{\alpha_c}$ as a function of the translational length ratio, $(V_l/V_g)^{1/3}$, between the vapor and liquid phase. The solid line in the inset is the prediction of the transition state theory (see Ref. 31).

Figure 15 shows results on the condensation coefficient $\overline{\alpha_c}$ for LJ monomers, dimers, and trimers. The agreement between results from the condensation probability and the velocity distributions is clear. Generally, $\overline{\alpha_c}$ decreases with a increasing T. For monomers in temperature range we could study, the reduction is approximately linear. The expected crossover in $\overline{\alpha_c}$ to unity at lower temperatures is not observed for monomers since at lower T the system crystallizes. But the crossover can be identified in the data from Ref. 38, which used the Dymond-Alder potential for argon in the low temperature range. For dimers and trimers, the expected crossover of $\overline{\alpha_c}$ to unity at lower temperatures is evident.

Figure 15 shows that the value of $\overline{\alpha_c}$ depends on the evaporation condition. This is obvious if we examine the monomer data at $T_b = 0.9\epsilon/k_B$. The value of $\overline{\alpha_c}$ at liquid/vapor equilibrium is slightly lower than its value at the evaporation rate $j_E = 2.5 \times 10^{-4}\tau^{-1}\sigma^{-2}$, and both are clearly lower than the value at the larger evaporation rate $j_E = 1.0 \times 10^{-3}\tau^{-1}\sigma^{-2}$.

However, if we take into account the fact that the temperature T_i of the liquid/vapor interface gets lower when evaporation is stronger and use T_i instead of T_b for the horizontal axis, all data fall nicely onto the same master curve indicated by the straight line in Fig. 15. The reason that $\overline{\alpha_c}$ is larger under stronger evaporation is that the interface temperature decreases due to evaporative cooling and lower temperature corresponds to larger $\overline{\alpha_c}$. This trend is also indicated by the data at $T_b = 1.0\epsilon/k_B$ for an equilibrium interface (thus $T_i = T_b$) and for a fixed evaporation rate $j_E = 2.5 \times 10^{-4}\tau^{-1}\sigma^{-2}$ (thus $T_i < T_b$). In the latter $\overline{\alpha_c}$ is found larger.

Our results show that the condensation coefficient $\overline{\alpha_c}$ is substantially less than unity for LJ monomers above the triple-point temperature, and is higher for LJ dimers and trimers at the same reduced temperature T/T_c. This is in contrast to the traditional viewpoint that the condensation coefficient decreases when the molecular composition changes from monatomic to polyatomic. In this viewpoint, the rotational motion of polyatomic molecules acts as a constraint to make the vapor condensation less likely. However, the short chain molecules we have simulated are very flexible. When two polyatomic molecules come into contact, their attractive interaction is stronger than that between two monatomic molecules because of the increase in the number of interacting sites. Furthermore, because of the flexibility, rotational degrees of freedom play a less important role. This leads to stronger cohesion for polyatomic chain molecules. It is therefore not surprising that $\overline{\alpha_c}$ is higher for LJ dimers and trimers at the same T/T_c because it basically represents how likely a molecule can bind to its liquid phase. Tsuruta and Nagayama also found that translational degrees of freedom dominate in the evaporation and condensation of water.[57]

Using transition state theory, Nagayama and Tsuruta derived a theoretical expression for $\overline{\alpha_c}$ in the case that the evaporation and condensation processes are dominated by translational motion of molecules.[31] In this framework, $\overline{\alpha_c}$ has a universal functional dependence on a translational length ratio, which is defined as the cubic root of the free volume ratio between the liquid and vapor phase, $(V_l/V_g)^{1/3}$. The results for $\overline{\alpha_c}$ versus $(V_l/V_g)^{1/3}$ are shown in the inset of Fig. 15. All data collapse onto a master curve except those for dimers at low temperature. However all data are above the theoretical line. Most data for $\overline{\alpha_c}$ in Ref. 31 are also above the theoretically predicted curve for $\overline{\alpha_c}$ vs. $(V_l/V_g)^{1/3}$.

VI. SUMMARY AND CONCLUSIONS

We have used MD simulations to investigate fluids made of LJ monomers, dimers, and trimers. The phase diagrams for the dimer and trimer systems were determined and their evaporation processes were simulated. Our results show that a simple change from monomer to dimer or trimer molecules has a strong effect on the evaporation rates. The evaporation rate of monomers when in contact with a vacuum is extremely high and there are strong evaporative cooling and liquid density enhancement near the liquid/vapor interface. All these effects are greatly reduced in dimer and trimer fluids. A physical explanation is provided on the basis that cohesion gets stronger for fluids made of longer chain molecules because of the increase in the number of interacting sites between two close molecules. The flexibility of the linear chain suppresses the importance of rotational motion of molecules, which tends to reduce the cohesion. The net outcome of the competition between these factors is that the surface tension is higher and the evaporation slows down at the liquid/vapor interface for fluids made of longer chains.

The measured evaporation rates for liquids evaporating into a vacuum were compared to the modified HK formula derived by Holyst and Litniewski. Good agreement was found for not only monatomic liquids composed of monomers, but also molecular liquids composed of dimers and trimers. It was confirmed that mechanical equilibrium, i.e., a constant component of the stagnation pressure normal to the liquid/vapor interface, holds for all systems at all times during evaporation. Furthermore, for liquids evaporating into vacuum, the momentum flux contribution dominates in the stagnation pressure in the vapor phase, which was first shown by Holyst and Litniewski to lead to the modified HK formula.[17]

Because of evaporative cooling, the temperature of the liquid/vapor interface is lower than the bulk temperature of liquid. It is further observed that the temperature increases in the vapor phase with the distance from the liquid/vapor interface. This makes the interface the coolest place in the system. The phenomenon that the vapor phase close to the interface has a temperature higher than that at the interface is qualitatively consistent with a previous experimental measurement on water.[19]

We measured velocity distributions of molecules at the liquid/vapor interface. As expected, in liquid/vapor equilibrium they follow the MB distribution. When the evaporation rate is controlled at a small value, the distribution also has a MB form but may correspond to a temperature that is slightly lower than the bulk temperature of either liquid or vapor phase. When a liquid evaporates into a vacuum, the molecules arriving at the interface have a velocity distribution that corresponds to a temperature much lower than that for the molecules leaving the interface. Furthermore, both temperatures are lower than the bulk temperature of the liquid phase far from the interface. In this case, evaporated molecules move away balistically in the vapor phase without encountering any impedance since the vapor density is extremely low. It is not surprising that local thermal equilibrium is not reached in this extreme situation. However, our data also showed that under moderate evaporation rates, which are usually the case in experiments, the vapor density remains comparable to its equilibrium value and the hypothesis of local thermal equilibrium becomes valid.

The condensation coefficient $\overline{\alpha_c}$ was determined by measuring the probability of reflection of molecules arriving at the liquid/vapor interface from the vapor phase. This probability generally depends on the normal component of the velocity of the arriving molecules. The functional form was confirmed to be exponential as in Eq. (11), consistent with the model of condensation probability of Tsuruta *et al.*.[29–32] Fitting the probability to Eq. (11) gave two parameters α and β, from which $\overline{\alpha_c}$ was calculated.

The apparent evaporation flux contains two contributions. One is from molecules that truly evaporate from the liquid phase, and another is from molecules arriving at the interface from the vapor phase but being reflected back. The velocity distributions of these two groups were measured and compared to modified MB distributions that depend on α and β. From these velocity distributions, α, β and eventually the condensation coefficient $\overline{\alpha_c}$ were also determined.

The condensation coefficients $\overline{\alpha_c}$ measured with the above two methods are very close, which serves as a validation of the kinetic model of Tsuruta *et al.*[29–32] We also found that $\overline{\alpha_c}$ decreases with increasing temperature T, consistent with the intuition that condensation becomes less likely at higher T. At the same reduced temperature T/T_c, trimer fluids have the largest $\overline{\alpha_c}$ and monomers have the smallest. This is in contrast to the traditional viewpoint that monatomic liquids have a condensation coefficient close to unity and polyatomic liquids have a value less than unity. However, since the chain molecules simulated here are very flexible, we do not think our results are in real contradiction with this viewpoint. The chain flexibility makes less prominent the rotational degrees of freedom that tend to frustrate the accommodation of incoming molecules to the liquid phase. Increasing in chain length leads to a stronger cohesive interaction between chain molecules. As a result, the condensation coefficient is higher for liquids made of molecules of longer chains. However, in most low molecular weight liquids, the molecules are relatively rigid, and the rotational motion plays a more important role in determining liquid cohesion and molecular orientation at the liquid/vapor interface. This can reduce the condensation coefficient, as suggested by some experiments. It remains an interesting open question to see if our observation that larger $\overline{\alpha_c}$ occurs for longer chains can be borne out by studying liquids made of a series of chain molecules such as hydrocarbons.

The condensation coefficients $\overline{\alpha_c}$ for monomers, dimers, and trimers almost collapse onto a single master curve when plotted against a translational length ratio, $(V_l/V_g)^{1/3}$, between the vapor and liquid phase. However, all of our data are consistently above the theoretical prediction of the model of Nagayama and Tsuruta based on transition state theory.[31] Note that V_l/V_g is just the inverse of the density ratio. This deviation indicates that the structure of a liquid/vapor interface is more complicated than that of a simple material-dividing plane characterized by a single parameter, $(V_l/V_g)^{1/3}$.

ACKNOWLEDGMENTS

This work was made possible by generous allocations of computer time at the New Mexico Computing Application Center NMCAC. This work is supported by the Laboratory Directed Research and Development program at Sandia National Laboratories. Sandia is a multiprogram laboratory operated by Sandia Corporation, a Lockheed Martin Company, for the United States Department of Energy under Contract No. DE-AC04-94AL85000.

[1] R. W. Schrage, *A Theoretical Study of Interphase Mass Transfer* (Columbia University Press, New York, 1953).
[2] Y. P. Pao, Phys. Fluids **14**, 306 (1971).
[3] Y. P. Pao, Phys. Fluids **14**, 1340 (1971).
[4] C. E. Siewert and J. R. Thomas, Jr., Phys. Fluids **16**, 1557 (1973).
[5] Y. Sone and Y. Onishi, J. Phys. Soc. Jpn **35**, 1773 (1973).
[6] Y. Sone, J. Phys. Soc. Jpn **45**, 315 (1978).
[7] J. W. Cipolla, Jr., H. Lang, and S. K. Loyalka, J. Chem. Phys. **61**, 69 (1974).
[8] D. A. Labuntsov and A. P. Kryukov, Int. J. Heat Mass Transfer **22**, 989 (1979).
[9] L. D. Koffman, M. S. Plesset, and L. Lees, Phys. Fluids **27**, 876 (1984).
[10] K. Aoki, Y. Sone, and T. Yamada, Phys. Fluids A **2**, 1867 (1990).
[11] D. Bedeaux, Adv. Chem. Phys. **64**, 47 (1986).
[12] D. Bedeaux and L. J. F. Hermans, Physica A **169**, 263 (1990).
[13] D. Bedeaux and S. Kjelstrup, Physica A **270**, 413 (1999).
[14] M. Bond and H. Struchtrup, Phys. Rev. E **70**, 061605 (2004).
[15] A. Frezzotti, L. Gibelli, and S. Lorenzani, Phys. Fluids **17**, 012102 (2005).
[16] R. Holyst and M. Litniewski, Phys. Rev. Lett. **100**, 055701 (2008).
[17] R. Holyst and M. Litniewski, J. Chem. Phys. **130**, 074707 (2009).
[18] J. P. Caputa and H. Struchtrup, Physica A **390**, 31 (2011).
[19] G. Fang and C. A. Ward, Phys. Rev. E **59**, 417 (1999).
[20] C. A. Ward and G. Fang, Phys. Rev. E **59**, 429 (1999).
[21] G. Fang and C. A. Ward, Phys. Rev. E **59**, 441 (1999).
[22] I. W. Eames, N. J. Marr, and H. Sabir, Int. J. Heat Mass Transfer **40**, 2963 (1997).
[23] R. Marek and J. Straub, Int. J. Heat Mass Transfer **44**, 39 (2001).
[24] M. Matsumoto and Y. Kataoka, J. Chem. Phys. **88**, 3233 (1988).
[25] M. Matsumoto and Y. Kataoka, J. Chem. Phys. **90**, 2398 (1989).
[26] M. Matsumoto and Y. Kataoka, Phys. Rev. Lett. **69**, 3782 (1992).
[27] K. Yasuoka, M. Matsumoto, and Y. Kataoka, J. Chem. Phys. **101**, 7904 (1994).
[28] M. Matsumoto, K. Yasuoka, and Y. Kataoka, J. Chem. Phys. **101**, 7912 (1994).
[29] T. Tsuruta, N. Sakamoto, and T. Masuoka, Therm. Sci. Eng. **3**, 85 (1995).
[30] T. Tsuruta, H. Tanaka, and T. Masuoka, Int. J. Heat Mass Transfer **42**, 4107 (1999).
[31] G. Nagayama and T. Tsuruta, J. Chem. Phys. **118**, 1392 (2003).
[32] T. Tsuruta and G. Nagayama, Energy **30**, 795 (2005).
[33] V. V. Zhaknovskii and S. I. Anisimov, Sov. Phys. JETP **84**, 734 (1997).
[34] S. I. Anisimov, D. O. Dunikov, V. V. Zhaknovskii, and S. P. Malyshenko, J. Chem. Phys. **110**, 8722 (1999).
[35] A. Rosjorde, D. W. Fossmo, D. Bedeaux, S. Kjelstrup, and B. Hafskjold, J. Colloid Interface Sci. **232**, 178 (2000).
[36] A. Rosjorde, S. Kjelstrup, D. Bedeaux, and B. Hafskjold, J. Colloid Interface Sci. **240**, 355 (2001).
[37] R. Meland, A. Frezzotti, T. Ytrehus, and B. Hafskjold, Phys. Fluids **16**, 223 (2004).
[38] T. Ishiyama, T. Yano, and S. Fujikawa, Phys. Fluids **16**, 2899 (2004).
[39] S. Fujikawa and M. Maerefat, JSME Int. J., Ser. II **33**, 634 (1990).
[40] K. Kremer and G. S. Grest, J. Chem. Phys. **92**, 5057 (1990).
[41] S. J. Plimpton, J. Comp. Phys. **117**, 1 (1995).
[42] See http://lammps.sandia.gov/.
[43] J. Cacas-Vázquez and D. Jou, Rep. Prog. Phys. **66**, 1937 (2003).
[44] M. J. P. Nijmeijer, A. F. Bakker, C. Bruin, and J. H. Sikkenk, J. Chem. Phys. **89**, 3789 (1988).
[45] P. Adams and J. R. Henderson, Mol. Phys. **73**, 1383 (1991).
[46] B. Smit, J. Chem. Phys. **96**, 8639 (1992).
[47] J. K. Johnson, J. A. Zollweg, and K. E. Gubbins, Mol. Phys. **78**, 591 (1993).
[48] N. B. Wilding, Phys. Rev. E **52**, 602 (1995).
[49] J. Potoff and A. Z. Panagiotopoulos, J. Chem. Phys. **109**, 10914 (1998).
[50] S. W. Sides, G. S. Grest, and M.-D. Lacasse, Phys. Rev. E **60**, 6708 (1999).
[51] W. Shi and J. K. Johnson, Fluid Phase Equilib. **187**, 171 (2001).
[52] J. G. Kirkwood and F. P. Buff, J. Chem. Phys. **17**, 338 (1949).
[53] J. Potoff and A. Z. Panagiotopoulos, J. Chem. Phys. **112**, 6411 (2000).
[54] M. P. Allen and D. J. Tildesley, *Computer Simulation of Liquids* (Clarendon Press, Oxford, 1987).
[55] J. Niknejad and J. W. Rose, Proc. R. Soc. London, Ser. A **378**, 305 (1981).
[56] D. C. Rapaport, *The Art of Molecular Dynamics Simulation* (Cambridge University Press, Cambridge, 1995).
[57] T. Tsuruta and G. Nagayama, J. Phys. Chem. B **108**, 1736 (2004).